# TsaP binds PilQ and is involved in cyclic di-GMP signaling

Matthew McCallum[1,2, †, ‡], Stephanie Tammam[1,†], John L. Rubinstein[1,2,3,*], Lori L. Burrows[4,*], P. Lynne Howell[1,2,*]

[1]Program in Molecular Structure & Function, Peter Gilgan Centre for Research and Learning, The Hospital for Sick Children, Toronto, ON M5G 0A4, Canada.

[2]Department of Biochemistry, University of Toronto, Toronto, ON M5S 1A8, Canada

[3]Department of Medical Biophysics, University of Toronto, Toronto, ON M5G 1l7, Canada.

[4]Department of Biochemistry and Biomedical Sciences and the Michael G. DeGroote Institute for Infectious Disease Research, McMaster University, Hamilton, ON L8S 4K1, Canada.

[*]To whom correspondence should be addressed:
howell@sickkids.ca, lori.burrows@mcmaster.ca, john.rubinstein@utoronto.ca

[†]These authors contributed equally to this work

[‡]Current address: Department of Biochemistry, University of Washington, Seattle, WA 98195-7350, USA.

## ABSTRACT

The type IV pilus machinery is a multi-protein complex that polymerizes and depolymerizes a pilus fibre used for attachment, twitching motility, phage adsorption, natural competence, protein secretion, and surface-sensing. An outer membrane secretin pore is required for passage of the pilus fibre out of the cell. Herein, the structure of the tetradecameric secretin, PilQ, from the *Pseudomonas aeruginosa* type IVa pilus was determined to 4.3 Å resolution in the presence and absence of $C_7$ symmetric spokes. The heptameric spokes were found to be the two tandem C-terminal domains of TsaP. TsaP forms a belt around PilQ and while the protein is not essential for PilQ assembly, over-expression of TsaP triggers the surface-sensing signal cascade upstream of PilY1, leading to cyclic di-GMP up-regulation. These results resolve the identity of the spokes identified with Proteobacterial PilQ and may reveal a new component of the surface-sensing cyclic di-GMP signal cascade.

## INTRODUCTION

The type IVa pilus (T4aP) facilitates many functions including attachment, twitching motility, phage adsorption, natural competence, protein secretion, and surface-sensing[1,2]. The surface-sensing role of T4aP is of particular interest due to its involvement in the up-regulation of cyclic di-GMP – the master regulator of biofilm formation[3,4]. Biofilms are of critical medical and industrial importance, as they increase bacterial tolerance of otherwise uninhabitable conditions, antibiotics, and the immune system[5]. The exact mechanism of T4aP-mediated surface sensing remains ambiguous, in part due to a lack of understanding in how the T4aP could transduce signals.

The T4aP machinery comprises an inner- and outer-membrane spanning multi-protein complex. This machinery polymerizes long thin fibres that attach to surfaces and retract to pull bacteria towards the point of attachment[1,2]. The pilus is a polymer mainly composed of the major subunit, PilA. At the pilus base, the inner membrane protein PilC is rotated by cytoplasmic ATPase motors, PilB and PilT, to catalyze polymerization and depolymerization, respectively[6,7]. Minor pilins and PilY1 prime pilus polymerization and are thus thought to localize to the pilus tip[8,9]. The pilus exits the periplasm through an outer membrane secretin, PilQ. Secretins often require chaperone proteins – known as pilotins – to shuttle secretin monomers from the inner membrane to the outer membrane and to facilitate secretin oligomerization[10]. PilF is the pilotin

50 for PilQ[11]. PilQ is aligned with the motors by a subcomplex of PilM, PilN, PilO, and PilP[12,13].
51 PilMNOP, PilY1, and PilT are all required for the T4aP surface sensing mechanism[14,15]. It is
52 unclear whether other proteins that are part of the T4aP apparatus that interface with PilM, PilN,
53 PilO, and PilP – such as PilQ – are also needed for surface sensing.
54 PilQ secretins from Proteobacteria, structurally characterized at low resolution, show
55 radial spokes emerging from a central barrel[16-19]. The identity of these spokes remains unknown,
56 although the spokes were suggested to be the peptidoglycan-binding component TsaP, shown to
57 be important for secretin spoke formation in *Neisseria sp.* and *Myxococcus xanthus*[16,19]. The
58 structures of the related type II secretion system (T2SS) secretins also have radial spokes[20,21].
59 These structures have been determined at 3-4 Å resolution, permitting modeling of the T2SS
60 pilotin spoke protein[20,21]. This finding suggests that the spokes in the T4aP structures could be the
61 T4aP pilotin, PilF, although PilF is structurally unrelated to the T2SS pilotin.
62 Secretins have a unique double-layered β-barrel architecture[22,23]. The outer β-barrel forms
63 a large vestibule that passes though the outer membrane[23]. The inner β-barrel curves inwards to
64 form a gate at the midway point of the outer β-barrel[23]. N1 and then N0 domains form rings
65 below the β-barrel[23]. In some secretins, additional N1-like domains form rings located between
66 the N1 ring and N0 ring[24], though PilQ from Proteobacteria typically lack these additional rings.
67 Instead, two or more septal peptidoglycan-binding AMI_N domains precede the N0 ring in
68 Proteobacterial PilQ[18,25]. Most secretins have a C-terminal S-domain following the β-barrel
69 region, though PilQ lacks this segment[26].
70 Recently models of PilQ from *Thermus thermophilus* ($PilQ^{Tt}$) and *Vibrio cholerae*
71 ($PilQ^{Vc}$) competence pilus systems were built into 7 and 2.7 Å resolution electron
72 cryomicroscopy (cryoEM) maps, respectively [27,28]. However, competence pilus PilQ secretins are
73 divergent from Proteobacterial T4aP PilQ secretins. Specifically, these secretins lack the lip
74 subdomain and the radial spokes. Instead, in the case of $PilQ^{Tt}$, extra density was identified where
75 the lip subdomains would be located[28].
76 We previously resolved a 7.4 Å map of PilQ from *Pseudomonas aeruginosa* ($PilQ^{Pa}$) with
77 presumed tetradecameric stoichiometry and $C_7$ symmetric spoke density[18]. Although at the time
78 this was the highest resolution structure of a secretin, it was not sufficient for model building.
79 Herein, our reprocessing of those micrographs with currently available image analysis and
80 model-building algorithms, yielded three distinct structures of $PilQ^{Pa}$. These maps were of

81 sufficient resolution to enable building of an atomic model. Mass spectrometry revealed the
82 identity of the protein bound in the spoke density to be TsaP, allowing a model to be built into the
83 spoke density. Functional characterization of the spoke protein supports a role for TsaP in the
84 surface-sensing signal cascade leading to cyclic di-GMP up-regulation.
85
86 **RESULTS**
87 **PilQ$^{Pa}$ forms tetradecameric and pentadecameric barrels**
88 We previously resolved a 7.4 Å resolution PilQ$^{Pa}$ cryoEM map[18]. Using the template-
89 based automatic particle selection algorithm implemented in cryoSPARC v.2[29], eight times more
90 particles were selected automatically from the original micrographs, where particle selection was
91 performed manually (**Supplementary Table 1**). Ab initio classification followed by
92 heterogeneous particle refinement in 3D revealed three unique classes, with 44 % of particle
93 images classified as $C_{14}$ symmetric barrels with $C_7$ symmetric radial spokes (**Figure 1A)**, 48 % of
94 particle images classifying as $C_{14}$ symmetric barrels without spokes (**Figure 1B)**, and 8 % as $C_{15}$
95 symmetric barrels without spokes (**Figure 1C**). Refining the three classes yielded maps at 4.3,
96 4.3, and 7.3 Å resolution, respectively. The distinct $C_{14}$ and $C_{15}$ symmetric maps identified are
97 reminiscent of the finding that the T2SS secretin can have more than one symmetry[24].
98 The map of the $C_{14}$ symmetric barrel with $C_7$ symmetric radial spokes had the best overall
99 map quality, with local resolution in the barrel estimated to be 3.5 Å. Secondary structure and
100 large side chains are visible, enabling model building of 14 PilQ$^{Pa}$ N1 and secretin domains
101 (**Figure 1A**). Although we verified that the AMI_N and N0 domains of PilQ were present using
102 mass spectrometry analyses (**Supplementary Figure 1**), they could not be modeled, consistent
103 with those domains adopting random orientations relative to the secretin barrel in the absence of
104 the peptidoglycan and the rest of the T4aP apparatus. Protomers of the barrel structure from the
105 spoked barrel map were fit into the maps of the $C_{14}$ and $C_{15}$ barrels without spokes and refined.
106 The final models were compared to co-evolved residues within PilQ$^{Pa}$ homologs as
107 identified by the EVcouplings webserver[30] (**Figure 1D**). There is a correlation between the co-
108 evolved residues and the N1 and secretin domains, validating these structures. The sequence of
109 the lip subdomain is not well conserved in PilQ (**Figure 1D**) consistent with the extracellular
110 exposure of this element. Consequently, poor sequence alignment in this region yields fewer co-
111 evolved residues in the lip subdomain. In the tetradecameric PilQ$^{Pa}$ maps (**Figure 1A-B**), the lip

112 subdomain appears folded open compared to lip subdomains from T2SS secretin structures[24,31].
113 Density for the lip in the C15 PilQ$^{Pa}$ barrel is absent (**Figure 1C**) suggesting it is disordered
114 relative to the secretin in this map.
115
116 **Co-evolved residues are consistent with secretin gate and barrel dynamics**
117 There are also co-evolved residues not directly supported by the model of PilQ$^{Pa}$. These
118 residues suggest dynamics not visualized in the cryoEM maps. There are co-evolved residues
119 between the secretin gate and the outer secretin barrel (**Figure 1E**). These co-evolved residues
120 are consistent with a model of secretin gate opening, as demonstrated recently for the secretin
121 from the type III secretion injectisome, InvG[32]. Co-evolved residues are also identified at the top
122 of the outer secretin barrel and near the bottom of the outer secretin barrel adjacent to the secretin
123 gate (**Figure 1F**). These co-evolved residues may be consistent with the outer secretin barrel
124 folding such that the top of the outer secretin barrel covers the gate-adjacent segment of the
125 secretin. The top of the secretin is hydrophobic (**Figure 1G**), like other secretin structures,
126 consistent with this region being the site for outer membrane insertion. Thus, one explanation for
127 these co-evolved residues may be that the outer secretin barrel forms a folding intermediate that
128 masks these sites prior to membrane insertion (**Figure 1F**). The gate-adjacent section of the outer
129 secretin barrel is highly conserved (**Figure 1G**) and provides the interface for the spoke density.
130 Thus, the spoke protein could bind this region to stabilize PilQ after outer-membrane insertion.
131
132 **Dynamics in the secretin gates visualized**
133 The conformations of the secretin gates in the $C_{15}$, $C_{14}$, and spoked $C_{14}$ PilQ$^{Pa}$ barrels are
134 different. While the secretin gate in the $C_{15}$ barrels is perpendicular to the walls of the barrel, the
135 secretin gate in the $C_{14}$ barrel invaginates towards the periplasm. Comparing the $C_{15}$ and $C_{14}$
136 barrels without spokes, the residues at the center of the secretin gate are displaced by 4 Å (**Figure**
137 **1B-C, Animation 1**). This invagination is likely the result of the 5 Å reduction in diameter of the
138 tetradecameric barrel relative to the pentadecameric form, leaving less room for the gate to
139 extend perpendicularly from the walls of the barrel.
140 Comparing the $C_{14}$ and spoked $C_{14}$ barrels reveals that the secretin gate invaginates by an
141 additional 3 Å in the spoked $C_{14}$ barrel (**Figure 1A-B**). A smaller barrel diameter cannot explain
142 this movement, as the diameters of the $C_{14}$ barrel and spoked $C_{14}$ barrels are identical. Comparing

143 the $C_{15}$, $C_{14}$, and spoked $C_{14}$ barrels reveals a pivot point for gate invagination in the outer barrel
144 adjacent to the secretin gate and the spokes (**Figure 1H-I and Animation 1**). This finding is
145 consistent with the molecules bound at the spokes promoting secretin gate invagination.
146
147 **TsaP co-purifies with PilQ**
148 There are two features in the maps of $PilQ^{Pa}$ that cannot be explained by models of $PilQ^{Pa}$
149 alone. First are the $C_7$ symmetric spokes. The spoke density appears to be comprised of 14
150 structurally similar β-roll protein structures that form a belt around PilQ. There are differences in
151 every other β-roll that give the spokes $C_7$ symmetry (**Figure 1A**). There is also extra density
152 beneath the secretin gate that plugs the small opening in the center of both tetradecameric PilQ
153 barrels – the density is more pronounced in the spoked tetradecameric barrel map (**Figure 1A-B**).
154 The local quality of the map beneath the secretin gate is too poor to identify distinct structural
155 elements. Curiously, there is no evidence of $C_{15}$ barrels with spokes or extra density beneath the
156 secretin gates, hinting at stoichiometry-dependent interactions.
157 To identify the protein(s) that constitute the extra densities, mass spectrometry was
158 performed on the protein sample used for cryoEM grid preparation. Aside from $PilQ^{Pa}$, the most
159 abundant components are PrpL, PA5122, and TsaP (**Supplementary Table 2, Supplementary**
160 **Figure 2**). TsaP is the protein most likely responsible for the spoke density as it has been shown
161 to be critical for PilQ spoke visualization in *Neisseria* sp. and *M. xanthus*[16,19]. PrpL is an
162 extracellular protease secreted by the T2SS[33,34] and thus unlikely to constitute these densities.
163 PA5122 is an uncharacterized protein with a secretion signal sequence.
164
165 **Model building of TsaP reveals unique heptamer structure**
166 The structure of TsaP is not known; however, TsaP is predicted to have an N-terminal
167 peptidoglycan-binding LysM domain linked by unstructured residues to a C-terminal domain.
168 The C-terminal domain of TsaP, henceforth referred to as the CII domain, is predicted to be
169 similar to the C-domain of the flagellar ring-forming component, FlgT[19]. The C-domain of FlgT
170 has a β-roll structure with an extruding finger subdomain[35]. The Phyre[2] predicted structure
171 prediction of TsaP from *P. aeruginosa* is consistent with this prediction (**Figure 2A**). To validate
172 this prediction, TsaP co-evolved residues identified by the EVcouplings webserver[30] were
173 compared with the predicted structure of the TsaP CII domain (**Figure 2B**). The correlations

174 between co-evolved residues and residues close to one another in the CII domain structure
175 prediction provide support for similarity of the predicted structure to the FlgT C-domain.
176 Inspection of TsaP co-evolved residues revealed a duplicate pattern of co-evolved residues
177 preceding the CII domain (**Figure 2B**), consistent with a second domain with a similar structure,
178 henceforth referred to as the CI domain. When the structure of the CI domain segment was
179 predicted[36,37] we found that it was also similar to the FlgT C-domain (**Figure 2A**). This is distinct
180 from previous predictions that have only identified a single C-domain in TsaP[19].
181 The β-roll structure and extruding finger subdomain in the CI and CII models can be
182 clearly seen in the spoke density (**Figure 2C**). There is also density consistent with linker
183 residues preceding the CI domain and between the CI and CII domains. In contrast, Phyre[2]
184 predicted structures of PrpL and PA5122 do not fit the size or shape of the spokes. The C-
185 terminal 224 residues of TsaP encompassing the CI and CII domains were therefore modeled and
186 refined into the map. This model reveals that TsaP forms a heptameric ring with $C_7$ symmetry
187 around $PilQ^{Pa}$ at the midpoint of the barrel where the internal gate is positioned (**Figure 2D**).
188 Each finger subdomain contacts the adjacent C domain to mediate intramolecular $CI^n$-$CII^n$
189 interactions and intermolecular $CII^n$-$CI^{n+1}$ interactions. These finger subdomain interactions
190 correlate with co-evolved residue pairs in TsaP (**Figure 2B**), further validating the model of TsaP
191 built into this map.
192 Each C domain contacts a unique PilQ protomer. The buried surface area of the TsaP-
193 PilQ interaction is 2924 $Å^2$ per TsaP protomer, or 20468 $Å^2$ for the entire 7:14 TsaP-PilQ
194 interaction. The buried surface area of the TsaP-TsaP oligomeric interface is 913 $Å^2$. The larger
195 buried surface area of the TsaP-PilQ interface compared with the TsaP-TsaP oligomeric interface
196 hints that the PilQ interaction may help facilitate TsaP oligomerization.
197
198 **Overexpression of TsaP triggers cyclic di-GMP signalling and biofilm formation**
199 We previously found that TsaP is not required for PilQ oligomerization, suggesting that
200 TsaP is not a pilotin[18]. *tsaP* mutants have a modest 40 % defect in twitching motility, which can
201 be complemented *in trans* with *tsaP* from an arabinose-inducible promotor without the addition
202 of arabinose (**Figure 3A**). Compared to the vector control, a 66 % defect in twitching motility is
203 observed in wild-type *P. aeruginosa* or the *tsaP* mutant complemented with *tsaP* when induced
204 with 0.1 % (w/v) arabinose – henceforth referred to as over-expressed TsaP. Intriguingly, when

205 TsaP is over-expressed there is qualitatively less crystal violet staining of adhered bacteria to the
206 polystyrene plates used in these twitching motility assays (**Figure 3B**).
207 As induction of cyclic di-GMP in *P. aeruginosa* yields biofilm matrixes with altered
208 adhesion properties[38], we hypothesised that TsaP overexpression may be altering cyclic di-GMP
209 levels. We therefore assessed the propensity of TsaP-overexpressing *P. aeruginosa* to form
210 biofilms using a Congo red dye uptake assay. Congo red binds to the Pel polysaccharide in *P.*
211 *aeruginosa* biofilms, leading to red colonies and a small clear halo around the colonies where the
212 dye has been taken up[39,40]. We found that the *tsaP* deletion mutant is indistinguishable from wild-
213 type *P. aeruginosa* (**Figure 3B**). However, TsaP overexpression in wild type or the *tsaP* mutant
214 lead to red colonies surrounded by pronounced clearing (**Figure 3B**), consistent with the over-
215 expression of TsaP leading to increased biofilm formation. Cyclic di-GMP induction has also
216 been implicated in reducing extracellular protease secretion[41,42]. We therefore assessed the
217 propensity of TsaP overexpressing *P. aeruginosa* to secrete proteases using a casein proteolysis
218 assay. Hydrolysis of casein by extracelluar proteases leads to clear halos around protease-
219 secreting colonies on solid skim milk media[43]. Clear halos form around wild-type *P. aeruginosa*
220 and the *tsaP* deletion mutant; however, no halos form around TsaP over-expressing colonies
221 (**Figure 3B**), consistent with TsaP overexpression leading to increased cyclic di-GMP and
222 decreased protease secretion. Finally, measurement of luciferase expression from a cyclic di-
223 GMP sensitive promotor verified that TsaP overexpression increases cellular cyclic di-GMP
224 concentrations (**Figure 3C**). Growth curves confirmed that increased luciferase expression is not
225 a result of increased cell growth: the cell density during the stationary phase of growth of bacteria
226 over-expressing TsaP is lower than wild type, consistent with resources being used for biofilm
227 formation instead of replication (**Figure 3C**). These results are consistent with TsaP being
228 involved with cyclic di-GMP signal modulation.
229
230 **TsaP signalling occurs upstream of PilY1**
231 Deletion of PilQ or the PilQ pilotin, PilF, does not prevent the over-expression of TsaP
232 from increasing Congo-red dye uptake (**Figure 3D**). This indicates that PilQ is not downstream
233 of TsaP in this signal cascade. PilY1 over-expression in *trans* can also trigger increased cyclic di-
234 GMP production[14]. To test whether TsaP over-expression triggers the signal cascade upstream of
235 PilY1, TsaP was over-expressed in a PilY1 deletion mutant. In this mutant, there is decreased

236 Congo-red dye uptake, consistent with TsaP over-expression inducing a signal cascade that
237 proceeds through PilY1 (**Figure 3D**). PilY1 induces a signalling cascade that proceeds through
238 PilM, PilN, PilO, and/or PilP, as deleting the *pilMNOP* genes blocks cyclic di-GMP induction
239 upon PilY1 over-expression[14]. Therefore, if TsaP over-expression indeed triggers the cyclic di-
240 GMP signal cascade upstream of PilY1, mutations in the *pilMNOP* genes should reduce cyclic
241 di-GMP signalling caused by TsaP over-expression. We found that TsaP over-expression in *pilN*,
242 *pilO*, or *pilP* mutants resulted in less Congo red dye uptake (**Figure 3D**), consistent with TsaP
243 triggering the same signal cascade as PilY1 to induce cyclic di-GMP.
244
245 **DISCUSSION**
246 We have determined the structure of PilQ alone and bound to TsaP at 4.3 Å resolution,
247 and demonstrated a role for TsaP in cyclic di-GMP signalling. Our results resolve the identity of
248 the spokes identified in Proteobacterial PilQ cryoEM densities and may reveal a new component
249 of the surface-sensing cyclic di-GMP signal cascade.
250 While most secretins are bound by their cognate pilotin around the periphery of the
251 secretin barrel adjacent to the secretin gate, we found $PilQ^{Pa}$ is bound by TsaP. Unlike the pilotin
252 PilF, TsaP is not essential for PilQ assembly or twitching motility[18]. Where and how PilF
253 interacts with PilQ remains an open question, although one possibility is that TsaP replaces PilF
254 after insertion of PilQ into the outer membrane (**Figure 4A**). We identified co-evolved residues
255 that are consistent with the TsaP-binding region of PilQ interacting with the hydrophobic
256 membrane-interacting interface. This hints at a model of PilQ membrane insertion in which
257 secretin monomers initially fold onto themselves with the TsaP-binding site occluding the
258 hydrophobic membrane insertion site. Binding by pilotins to the TsaP-binding site might then
259 stabilize membrane-embedded PilQ, rationalizing the necessity of pilotins for secretin assembly
260 and localization. If this were the case, after outer-membrane insertion of PilQ, PilF would be
261 replaced with TsaP in *P. aeruginosa* (**Figure 4A**).
262 The co-structure of TsaP and PilQ provides hints about the functional role of TsaP. The
263 structure of PilQ was determined in two distinct stoichiometries. Interestingly, only the
264 tetradecameric form is bound by TsaP and the unidentified secretin gate plug. Likewise, the 2:1
265 PilQ:TsaP configuration necessitates binding of only even-numbered PilQ stoichiometries. It may
266 be TsaP recognizes or selects for specific secretin stoichiometries. Selecting particular secretin

267 stoichiometries may improve the efficiency of T4aP function, consistent with the moderate
268 twitching motility defect of the TsaP-deletion mutant.
269 Alternatively, TsaP binding PilQ could alter the tertiary structure of PilQ. Comparing the
270 different PilQ structures reveals a pivot point for secretin gate invagination adjacent to the
271 spokes, consistent with TsaP binding influencing this process (**Figure 4B**). Thus, a possible role
272 for TsaP may be in modifying secretin-gate invagination. TsaP could also be involved with much
273 larger-scale secretin movements. For example, PilQ adopts distinct states depending on whether
274 the pilus fibre occupies the central channel the T4aP[19,27]. Compared to T4aP maps obtained by
275 electron cryotomography in which the pilus fibre does not occupy the T4aP, the OM in the
276 piliated state has moved 20Å away from PilP and the peptidoglycan[19]. Although the secretin
277 domain is embedded in the OM, the AMI_N and N0 domains of PilQ bind peptidoglycan and
278 PilP, respectively[25]. This suggests that PilQ must extend and contract when going between the
279 piliated and non-piliated states. As TsaP binds to both the peptidoglycan and secretin domain of
280 PilQ, TsaP binding could prevent secretins from adopting an open state (**Figure 4C**). In other
281 words, TsaP could act as an elastic band between the peptidoglycan and outer-membrane
282 components of PilQ, keeping PilQ contracted and the T4aP closed in the absence of an assembled
283 pilus. The predicted disordered residues between the LysM and CI/CII domains could afford
284 TsaP the elasticity required for this action.
285 Altered conformation of PilQ might be sensed by other PilQ-binding proteins, such as
286 PilP binding to the N0 domain of PilQ or the plug protein located beneath the secretin gates.
287 However, it appears that PilQ is not downstream of TsaP cyclic di-GMP signalling, as deletion of
288 PilQ does not interrupt the increased Congo Red dye binding upon TsaP overexpression. This is
289 curious as PilQ provides the only known physical contact between TsaP and PilN, PilO, and PilP
290 – which are important for inducing cyclic di-GMP production. This suggests there is a PilQ-
291 independent signal transduction pathway from TsaP to PilY1 and PilNOP. It is worth noting that
292 PilN, PilO, and PilP are mutually dependent on each other for stability[44], so deleting one gene
293 can reduce expression of all three. Therefore, it may be that the signal transduction pathway
294 proceeds through only one of PilN, PilO, or PilP.
295 It seems likely that TsaP and PilQ are tightly associated, as the buried surface area of the
296 TsaP-PilQ interaction is enormous (20468 $Å^2$) and stable in detergent. It is nonetheless possible
297 that some of the TsaP was removed during the purification as only about half of the purified PilQ

298 particles have TsaP associated with them. Alternatively, there may be a population of free PilQ
299 and TsaP in the cell. These unbound proteins may be an intermediate state between PilQ-PilF and
300 PilQ-TsaP complexes. Given that TsaP over-expression triggers cyclic di-GMP induction
301 independent of PilQ, the unbound population of TsaP may trigger signalling. Alternatively, TsaP
302 could be downstream of PilQ in the cyclic di-GMP signal cascade. For example, under native
303 expression conditions conformational changes in PilQ could trigger TsaP binding and nucleate
304 TsaP oligomerization, and this oligomerization could be the trigger for cyclic di-GMP signalling.
305 In this case, over-expressed TsaP could signal for increased cyclic di-GMP if TsaP spontaneously
306 oligomerizes when over-expressed (**Figure 4D**). At present, the exact mechanism of how TsaP
307 initiates and relays a signal through PilY1 and PilNOP for cyclic di-GMP remains a tantalizing
308 mystery.
309
310 **METHODS**
311 **Cloning and mutagenesis**
312 TsaP from *P. aeruginosa* PAO1 was PCR amplified from genomic DNA using primers
313 TsaP_fwd and TsaP_rev (**Supplementary Table 3**), digested with KpnI and XbaI, and cloned into
314 pBADGr to create pBADGr:*tsaP* for arabinose inducible expression of TsaP. Plasmid sequences
315 were verified by TCAG sequencing facilities (The Hospital for Sick Children, Canada).
316
317 **TsaP Deletion**
318 A gene deletion allele was ordered from BioBasic and subcloned into pEX18Gm at the
319 BamHI site producing pEX18Gm_*tsaP*. Clones were confirmed by digest and DNA sequencing
320 (TCAG, The Hospital for Sick Children). The pEX18Gm_*tsaP* construct was transformed into
321 chemically competent SM10 *E. coli* cells, colonies containing pEX18Gm_*tsaP* were mated with
322 mPAO1 using a method described elsewhere[49]. Briefly, after mating *P. aeruginosa* was selected
323 for by growth on LB agar plates containing 25 μg/ml triclosan (Sigma) followed by selection of
324 the merodiploid strains on VBMM agar containing 30 μg/ml gentamicin. Counter selection to
325 resolve the merodiploids was performed on 1.5 % agar plates with 10 g/L tryptone, 5 g/L yeast
326 extract, and 15% (wt/vol) sucrose. The deletion was verified by the absence of a PCR product using
327 primers TsaP_fwd and TsaP_rev.
328

329 **Phenotypic characterizations**

330 *P. aeruginosa* PAO1 with and without deletion mutations of *tsaP*, *pilN*, *pilO*, *pilP*, *pilQ*,
331 *pilY1* were electroporated with pBADGr or pBADGr:tsaP. *P. aeruginosa* PAO1 with and without
332 deletion mutations of *tsaP* were also electroporated with pBADGr:tsaP.

333 Twitching assays were performed as described previously[50,51] except that assays were
334 performed in 150 mm by 15 mm petri polystyrene dishes (Fisher Scientific) with 30 µg/ml
335 gentamicin for 18 h at 37 °C. After this incubation, the agar was then carefully discarded and the
336 adherent bacteria were stained with 1 % (w/v) crystal violet dye, followed by washing with
337 deionized water to remove unbound dye. Twitching zone areas were measured using ImageJ
338 software[52]. Twitching motility assays were performed in six replicates.

339 For Congo-red dye binding assays, cells were grown in 0.5 mL of lysogeny broth (LB) with
340 30 µg/ml gentamicin for 16 h at 37 °C while shaking. Cultures were normalized to an OD at 600
341 nm of 0.1 and then 3 µl of culture was spotted onto Congo red plates (1% (wt/vol) Tryptone, 1%
342 (wt/vol) agar, 0.004% (wt/vol) congo red, and 0.0015% (wt/vol) Coomassie Brilliant Blue R250,
343 and either 0, 0.01, or 0.1% L-arabinose) with the appropriate antibiotic, and grown for 24-36 h at
344 37 °C.

345 Extracellular proteases were assayed using skim milk plates (1% wt/vol agar, 1% wt/vol
346 skim milk powder, and either 0, 0.01, or 0.1% L-arabinose) with the appropriate antibiotic, using
347 the same normalized cultures used for the Congo red binding assays. 3 µl of culture was spotted
348 on a plate and incubated for 16 hrs at 37 °C. All plates were scanned using an Epson Perfection
349 4990 scanner and Epson Scan software.

350 For luciferase expression, cells previously electroporated with pBADGr, pBADGr::tsaP
351 and pBADGr::tsaP mutant constructs were electroporated with pMS402:PcdrA. Cells were grown
352 in 0.5 mL of lysogeny broth (LB) with 30 µg/ml gentamicin and 150 µg/ml kanamycin for 16 h at
353 37 °C while shaking. Cultures were normalized to OD600 of 0.1 and diluted 10x into fresh LB
354 broth containing 30 µg/ml gentamicin, 105 µg/ml kanamycin and either 0, 0.01% or 0.1% L-
355 arabinose in a 384 well plate (Corning, 3821). All samples were done in triplicate. Growth and
356 luciferase activity were monitored over a 16-hour period in a Synergy Neo2 plate reader (BioTek
357 Instruments). Data was analyzed and plotted using Prism 8 (Graph Pad).

358

359 **Plotting the residues at the packing unit interface**

360 CMview[53] was used to identify residues that are near one another. The contact type was set
361 to 'ALL' (i.e. every atom available in the structure) and the distance cut-off was set to 8 Å. To
362 identify residues that are near one another in PilQ monomers, the CI domain of TsaP (residues 126-
363 211), or the CII domain of TsaP (residues 235-324), these structure segments were loaded
364 separately. To identify intra-molecular CI to CII residues that are near each other in TsaP, full-
365 length TsaP was loaded. To identify inter-molecular residues that are near one another, two
366 adjacent PilQ protomers were loaded together, or the CI domain and CII domains from two adjacent
367 protomers were loaded together.
368
369 **Identifying evolutionarily-coupled residues**
370 The TsaP and PilQ$^{Pa}$ amino acid sequences were analyzed using the EVcouplings
371 webserver[30] with default parameters. Homologs were identified, aligned, and analyzed – in total,
372 2642 and 11302 for TsaP and PilQ, respectively. There was poor alignment quality in the lip
373 subdomain of PilQ (residues 481-531) so few evolutionarily-coupled residue pairs were discovered
374 in the lip subdomain. Only residue pairs with a probability score greater than 0.845 or 0.985 were
375 included in subsequent analysis, for TsaP and PilQ, respectively. To better understand the
376 significance of these evolutionarily coupled residues, they were compared to the residues that are
377 near one another identified in CMview.
378
379 **CryoEM analysis**
380 As previously described for this dataset[18], cryoEM data was collected as movies (30 frames
381 over 15 sec) with a FEI Tecnai F20 electron microscope operating at 200 kV and equipped with a
382 Gatan K2 Summit direct detector camera. The exposure rate was 5 electrons/pixel/s with a
383 calibrated pixel size of 1.45 Å/pixel. Movie frames were aligned with an implementation of
384 alignframes_lmbfgs[54] within cryoSPARC v2.8.0. All subsequent image processing was performed
385 in cryoSPARC v2.8.0[29] (**Supplementary Table 1**). CTF parameters were estimated from the
386 average of aligned frames with CTFFIND4[55] within cryoSPARC and individual particle motion
387 correction and exposure weighting was done with an implementation of alignparts_lmbfgs[54] within
388 cryoSPARC. Initial 2D class averages were generated with manually selected particle images;
389 these class averages were then used to select more particle images. Particle images were extracted
390 in 256×256 pixel boxes then subjected to 2D classification. For the purposes of 3D classification,

391 particle images contributing to 2D classes without high-resolution features were removed. *Ab initio*
392 reconstruction was performed using two classes, revealing barrels and spoked-barrels. The particles
393 contributing to the barrels without spokes were used for an additional round of *ab initio*
394 reconstruction with two classes, revealing an additional class with wider barrels. The spoked
395 barrels, the barrels without spokes, and the wider barrels without spokes were then used as initial
396 models for heterogeneous refinement; particles from 3D classes that did not converge at this stage
397 were removed. Particles from distinct 3D classes were then subjected to non-uniform refinement[56].
398 A molecular model could be built using Coot[57] into the spoked barrel map using the
399 structures of FlgT and GspD[24,35] as guides for TsaP and PilQ, respectively. Molecular models for
400 the maps of barrels without spokes were built by fitting the PilQ protomers built into the spoked
401 barrel map in Coot[57]. These models were refined against the maps in Phenix-Refine[58] with
402 reference model restraints to the spoked barrel PilQ structures. While side-chains were used to
403 ensure the models made biological sense during model building, they were ultimately removed as
404 the map quality did not justify them being modeled.
405
406
407 **Acknowledgements**
408 This work was supported by a grant from the Canadian Institutes for Health Research (CIHR) MOP
409 93585 to L.L.B. and P.L.H. M.M. was supported by a CIHR Doctoral Studentship and Ontario
410 Graduate Scholarship during these studies. P.L.H. and J.L.R. are recipients of Canada Research
411 Chairs. The graphics programs used in this study were accessed using SBGrid.
412
413
414 **REFERENCES**
415 1. McCallum, M., Burrows, L.L. & Howell, P.L. The Dynamic Structures of the Type IV
416 Pilus. *Microbiol Spectrum* **7**(2019).
417 2. Craig, L., Forest, K.T. & Maier, B. Type IV pili: dynamics, biophysics and functional
418 consequences. *Nat Rev Microbiol* **17**, 429-440 (2019).
419 3. Chang, C.Y. Surface Sensing for Biofilm Formation in Pseudomonas aeruginosa. *Front*
420 *Microbiol* **8**, 2671 (2017).
421 4. Valentini, M. & Filloux, A. Biofilms and Cyclic di-GMP (c-di-GMP) Signaling: Lessons
422 from Pseudomonas aeruginosa and Other Bacteria. *J Biol Chem* **291**, 12547-55 (2016).
423 5. Mah, T.F. & O'Toole, G.A. Mechanisms of biofilm resistance to antimicrobial agents.
424 *Trends Microbiol* **9**, 34-9 (2001).

425 6. McCallum, M., Tammam, S., Khan, A., Burrows, L.L. & Howell, P.L. The molecular
426 mechanism of the type IVa pilus motors. *Nat Commun* **8**, 15091 (2017).
427 7. McCallum, M. et al. Multiple conformations facilitate PilT function in the type IV pilus.
428 *Nat Commun* **10**, 5198 (2019).
429 8. Marko, V.A., Kilmury, S.L.N., MacNeil, L.T. & Burrows, L.L. Pseudomonas aeruginosa
430 type IV minor pilins and PilY1 regulate virulence by modulating FimS-AlgR activity.
431 *PLoS Pathog* **14**, e1007074 (2018).
432 9. Nguyen, Y. et al. Pseudomonas aeruginosa minor pilins prime type IVa pilus assembly
433 and promote surface display of the PilY1 adhesin. *J Biol Chem* **290**, 601-11 (2015).
434 10. Koo, J., Burrows, L.L. & Howell, P.L. Decoding the roles of pilotins and accessory
435 proteins in secretin escort services. *FEMS Microbiol Lett* **328**, 1-12 (2012).
436 11. Koo, J. et al. PilF is an outer membrane lipoprotein required for multimerization and
437 localization of the Pseudomonas aeruginosa Type IV pilus secretin. *J Bacteriol* **190**,
438 6961-9 (2008).
439 12. McCallum, M. et al. PilN Binding Modulates the Structure and Binding Partners of the
440 Pseudomonas aeruginosa Type IVa Pilus Protein PilM. *J Biol Chem* **291**, 11003-15
441 (2016).
442 13. Tammam, S. et al. PilMNOPQ from the Pseudomonas aeruginosa type IV pilus system
443 form a transenvelope protein interaction network that interacts with PilA. *J Bacteriol* **195**,
444 2126-35 (2013).
445 14. Luo, Y. et al. A hierarchical cascade of second messengers regulates Pseudomonas
446 aeruginosa surface behaviors. *mBio* **6**(2015).
447 15. Persat, A., Inclan, Y.F., Engel, J.N., Stone, H.A. & Gitai, Z. Type IV pili
448 mechanochemically regulate virulence factors in Pseudomonas aeruginosa. *Proc Natl*
449 *Acad Sci U S A* **112**, 7563-8 (2015).
450 16. Siewering, K. et al. Peptidoglycan-binding protein TsaP functions in surface assembly of
451 type IV pili. *Proc Natl Acad Sci U S A* **111**, E953-61 (2014).
452 17. Collins, R.F. et al. Structure of the Neisseria meningitidis outer membrane PilQ secretin
453 complex at 12 A resolution. *J Biol Chem* **279**, 39750-6 (2004).
454 18. Koo, J., Lamers, R.P., Rubinstein, J.L., Burrows, L.L. & Howell, P.L. Structure of the
455 Pseudomonas aeruginosa Type IVa Pilus Secretin at 7.4 A. *Structure* **24**, 1778-1787
456 (2016).
457 19. Chang, Y.W. et al. Architecture of the type IVa pilus machine. *Science* **351**, aad2001
458 (2016).
459 20. Yin, M., Yan, Z. & Li, X. Structural insight into the assembly of the type II secretion
460 system pilotin-secretin complex from enterotoxigenic Escherichia coli. *Nat Microbiol* **3**,
461 581-587 (2018).
462 21. Chernyatina, A.A. & Low, H.H. Core architecture of a bacterial type II secretion system.
463 *Nat Commun* **10**, 5437 (2019).
464 22. Filloux, A. & Voulhoux, R. Multiple Structures Disclose the Secretins' Secrets. *J*
465 *Bacteriol* **200**(2018).
466 23. Worrall, L.J. et al. Near-atomic-resolution cryo-EM analysis of the Salmonella T3S
467 injectisome basal body. *Nature* **540**, 597-601 (2016).
468 24. Yan, Z., Yin, M., Xu, D., Zhu, Y. & Li, X. Structural insights into the secretin
469 translocation channel in the type II secretion system. *Nat Struct Mol Biol* **24**, 177-183
470 (2017).

471 25. Berry, J.L. et al. Structure and assembly of a trans-periplasmic channel for type IV pili in
472 Neisseria meningitidis. *PLoS Pathog* **8**, e1002923 (2012).
473 26. Majewski, D.D., Worrall, L.J. & Strynadka, N.C. Secretins revealed: structural insights
474 into the giant gated outer membrane portals of bacteria. *Curr Opin Struct Biol* **51**, 61-72
475 (2018).
476 27. Weaver, S.J., Sazinsky, M.H., Dalia, T.N., Dalia, A.B. & Jensen, G.J. CryoEM structure
477 of the Vibrio cholerae Type IV competence pilus secretin PilQ. *bioRxiv* (2020).
478 28. D'Imprima, E. et al. Cryo-EM structure of the bifunctional secretin complex of Thermus
479 thermophilus. *Elife* **6**, e30483 (2017).
480 29. Punjani, A., Rubinstein, J.L., Fleet, D.J. & Brubaker, M.A. cryoSPARC: algorithms for
481 rapid unsupervised cryo-EM structure determination. *Nat Methods* **14**, 290-296 (2017).
482 30. Marks, D.S. et al. Protein 3D structure computed from evolutionary sequence variation.
483 *PLoS One* **6**, e28766 (2011).
484 31. Hay, I.D., Belousoff, M.J. & Lithgow, T. Structural Basis of Type 2 Secretion System
485 Engagement between the Inner and Outer Bacterial Membranes. *MBio* **8**, e01344-17
486 (2017).
487 32. Hu, J. et al. Cryo-EM analysis of the T3S injectisome reveals the structure of the needle
488 and open secretin. *Nat Commun* **9**, 3840 (2018).
489 33. Wilderman, P.J. et al. Characterization of an endoprotease (PrpL) encoded by a PvdS-
490 regulated gene in Pseudomonas aeruginosa. *Infect Immun* **69**, 5385-94 (2001).
491 34. Michel, G.P., Durand, E. & Filloux, A. XphA/XqhA, a novel GspCD subunit for type II
492 secretion in Pseudomonas aeruginosa. *J Bacteriol* **189**, 3776-83 (2007).
493 35. Terashima, H. et al. Insight into the assembly mechanism in the supramolecular rings of
494 the sodium-driven Vibrio flagellar motor from the structure of FlgT. *Proc Natl Acad Sci*
495 *U S A* **110**, 6133-8 (2013).
496 36. Kelley, L.A., Mezulis, S., Yates, C.M., Wass, M.N. & Sternberg, M.J. The Phyre2 web
497 portal for protein modeling, prediction and analysis. *Nat Protoc* **10**, 845-58 (2015).
498 37. Yang, J. et al. The I-TASSER Suite: protein structure and function prediction. *Nat*
499 *Methods* **12**, 7-8 (2015).
500 38. Ha, D.G. & O'Toole, G.A. c-di-GMP and its Effects on Biofilm Formation and
501 Dispersion: a Pseudomonas Aeruginosa Review. *Microbiol Spectr* **3**, MB-0003-2014
502 (2015).
503 39. Jones, C.J. & Wozniak, D.J. Congo Red Stain Identifies Matrix Overproduction and Is an
504 Indirect Measurement for c-di-GMP in Many Species of Bacteria. *Methods Mol Biol*
505 **1657**, 147-156 (2017).
506 40. Vasseur, P., Vallet-Gely, I., Soscia, C., Genin, S. & Filloux, A. The pel genes of the
507 Pseudomonas aeruginosa PAK strain are involved at early and late stages of biofilm
508 formation. *Microbiology* **151**, 985-997 (2005).
509 41. Ravichandran, A., Ramachandran, M., Suriyanarayanan, T., Wong, C.C. & Swarup, S.
510 Global Regulator MorA Affects Virulence-Associated Protease Secretion in Pseudomonas
511 aeruginosa PAO1. *PLoS One* **10**, e0123805 (2015).
512 42. Lopez-Baena, F.J., Vinardell, J.M. & Medina, C. Regulation of Protein Secretion Systems
513 Mediated by Cyclic Diguanylate in Plant-Interacting Bacteria. *Front Microbiol* **10**, 1289
514 (2019).
515 43. Sokol, P.A., Ohman, D.E. & Iglewski, B.H. A more sensitive plate assay for detection of
516 protease production by Pseudomanas aeruginosa. *J Clin Microbiol* **9**, 538-40 (1979).

517 44. Ayers, M. et al. PilM/N/O/P proteins form an inner membrane complex that affects the
518 stability of the Pseudomonas aeruginosa type IV pilus secretin. *J Mol Biol* **394**, 128-42
519 (2009).
520 45. Chen, V.B. et al. MolProbity: all-atom structure validation for macromolecular
521 crystallography. *Acta Crystallogr D Biol Crystallogr* **66**, 12-21 (2010).
522 46. Jacobs, M.A. et al. Comprehensive transposon mutant library of Pseudomonas
523 aeruginosa. *Proc Natl Acad Sci U S A* **100**, 14339-44 (2003).
524 47. Koo, J. et al. Functional mapping of PilF and PilQ in the Pseudomonas aeruginosa type
525 IV pilus system. *Biochemistry* **52**, 2914-23 (2013).
526 48. Asikyan, M.L., Kus, J.V. & Burrows, L.L. Novel proteins that modulate type IV pilus
527 retraction dynamics in Pseudomonas aeruginosa. *J Bacteriol* **190**, 7022-34 (2008).
528 49. de Lorenzo, V. & Timmis, K.N. Analysis and construction of stable phenotypes in gram-
529 negative bacteria with Tn5- and Tn10-derived minitransposons. *Methods Enzymol* **235**,
530 386-405 (1994).
531 50. Ha, D.G., Kuchma, S.L. & O'Toole, G.A. Plate-based assay for swarming motility in
532 Pseudomonas aeruginosa. *Methods Mol Biol* **1149**, 67-72 (2014).
533 51. Turnbull, L. & Whitchurch, C.B. Motility assay: twitching motility. *Methods Mol Biol*
534 **1149**, 73-86 (2014).
535 52. Schneider, C.A., Rasband, W.S. & Eliceiri, K.W. NIH Image to ImageJ: 25 years of
536 image analysis. *Nat Methods* **9**, 671-5 (2012).
537 53. Vehlow, C. et al. CMView: interactive contact map visualization and analysis.
538 *Bioinformatics* **27**, 1573-4 (2011).
539 54. Rubinstein, J.L. & Brubaker, M.A. Alignment of cryo-EM movies of individual particles
540 by optimization of image translations. *J Struct Biol* **192**, 188-95 (2015).
541 55. Rohou, A. & Grigorieff, N. CTFFIND4: Fast and accurate defocus estimation from
542 electron micrographs. *J Struct Biol* **192**, 216-21 (2015).
543 56. Punjani, A., Zhang, H., Fleet D. J. Non-uniform refinement: Adaptive regularization
544 improves single particle cryo-EM reconstruction. *bioRxiv* (2019).
545 57. Casanal, A., Lohkamp, B. & Emsley, P. Current Developments in Coot for
546 Macromolecular Model Building of Electron Cryo-microscopy and Crystallographic
547 Data. *Protein Sci* (2019).
548 58. Afonine, P.V. et al. Real-space refinement in PHENIX for cryo-EM and crystallography.
549 *Acta Crystallogr D Struct Biol* **74**, 531-544 (2018).
550

551

552 **Figure Legends**

553 **Figure 1. Electron cryomicroscopy of PilQ from *P. aeruginosa* reveals multiple conformers.**

554 **A-C,** Map (upper left) and model (upper right) of $PilQ^{Pa}$ (coloured) with additional spoke and

555 plug density (black). Top (top), side (middle), and cross section (bottom) views are shown. **A,**

556 Map and model of spoked tetradecameric $PilQ^{Pa}$ (purple). **B,** Map and model of tetradecameric

557 $PilQ^{Pa}$ without spokes (teal). **C,** Map and model of pentadecameric $PilQ^{Pa}$ (orange). **D,**

558 Evolutionarily coupled residues in PilQ (gray) are compared with the structure of $PilQ^{Pa}$. Residue

559 pairs that are within 8 Å of each other in the tertiary structure of PilQ$^{Pa}$ are shown (black).
560 Residue pairs that are within 8 Å of each other between PilQ$^{Pa}$ protomers are also shown (gold).
561 Specific evolutionarily coupled residues that are not supported by the PilQ$^{Pa}$ structure are noted
562 with coloured arrows: G554-P635 (yellow), E663-A624 (red), T538-E652 (green), L545-T653
563 (magenta), and L546-V457 (blue). **E**, Location of the G554-P635 and E663-A624 residue pairs
564 on a cross section of PilQ$^{Pa}$ (left) and a model for secretin gate opening consistent with these co-
565 evolved residues. **F**, Location of the T538-E652, L545-T653, and L546-V457 residue pairs on
566 PilQ$^{Pa}$ (left) and a model for outer-barrel folding consistent with these co-evolved residues. **G,**
567 Surface representation of conserved residues (top) and electrostatic potential (bottom) in PilQ$^{Pa}$.
568 **H,** Structure alignment of monomers from the spoked tetradecameric PilQ$^{Pa}$ (purple),
569 tetradecameric PilQ$^{Pa}$ with no spokes (teal), and pentadecameric PilQ$^{Pa}$ (orange) models. Grey
570 square with black PilQ cartoon has a dotted red box highlighting area of PilQ shown. Structural
571 differences are highlighted (arrows) and the pivot point for these differences is noted (black
572 circle). **I,** Cartoon model summarizing the differences between the three PilQ$^{Pa}$ structures
573 determined. Pentadecameric PilQ$^{Pa}$ (orange) is wider and has more horizontal secretin gates
574 compared to the other structures. Tetradecameric PilQ$^{Pa}$ (teal) has invaginated secretin gates and
575 partial plug density (black triangle). Spoked tetradecameric PilQ$^{Pa}$ (purple) has further
576 invaginated secretin gates, plug density (black triangle), and spokes (black circles).
577
578 **Figure 2. TsaP can be modeled in the PilQ spoke density as a heptameric ring. A,** TsaP
579 domain model predictions: the I-Tasser prediction of the CI domain (residues 126-211)[37] and the
580 Phyre[2] prediction of the CII domain (residues 235-324)[36]. **B,** Evolutionarily coupled residues in
581 TsaP (gray) are compared with the structure of the C-terminal 224 residues of TsaP. Residue
582 pairs that are within 8 Å of each other are shown from the CI domain (yellow), the CII domain
583 (wheat-yellow), and the linkers preceding and following the CI domain (brown). Intramolecular
584 and intermolecular contacts in the TsaP structure between the CI and CII domains are also shown
585 (blue and red, respectively). **C-D,** Map (top), model (middle), and cartoon (bottom) summarizing
586 the structure of TsaP. Zoomed-in (**C**) and zoomed-out (**D**) views are shown. TsaP is coloured as
587 in **B**; PilQ is shown in grey (**C**) or purple (**D**).
588

589 **Figure 3. TsaP over-expression induces cyclic di-GMP up-regulation.** Wild-type *P. aeruginosa*
590 (left), the *tsaP* mutant (center left), *P. aeruginosa* expressing TsaP (center right), and the *tsaP*
591 mutant expressing TsaP (right). **A,** Twitching motility was assayed by crystal violet staining and
592 the areas traversed by the bacteria were measured (violin plot, n = 6). Mean twitching areas were
593 compared to wild type plus the control vector with the two-way ANOVA test; reported p-values
594 were less than 0.01 (*) or 0.0001 (***). **B**, Representative (?) Crystal violet stained twitching
595 motility zones (top), Congo-red agar colonies (middle), and skim milk agar colonies (bottom) are
596 shown for 0 % arabinose induction (-) or 0.1% arabinose induction (++). **C**, Luminescence over
597 time relative to uninduced control without arabinose (top), with luciferase expression under the
598 control of the cyclic di-GMP inducible *cdrA* promotor. Mean luminescence relative to a matched
599 uninduced control (n=3) is shown for 0.1% arabinose induction (orange, ++) or 0.01% arabinose
600 induction (beige, +) as a filled in line with the standard error of the mean (SEM) (dotted lines).
601 Growth measured by absorbance at 600nm over time of liquid cultures (bottom). Mean growth
602 (n=3) is shown for 0 % arabinose induction (gray, -), 0.01% arabinose induction (beige, +), or 0.1
603 % arabinose induction (orange, ++) with the SEM shown (dotted lines). **D**, Congo red dye uptake
604 assay of PAO1 (wild-type), PAO1::*pilN*, PAO1::*pilO*, PAO1::*pilP*, PAO1::*pilQ*, PAO1::*pilA*,
605 PAO1::*pilF* and PAO1::*pilY1* with (++) and without (-) TsaP overexpression.
606
607 **Figure 4. Potential molecular functions of TsaP. A,** The outer-barrel of PilQ (purple) adjacent
608 to the secretin gate may conceal the hydrophobic membrane proximal section until membrane
609 insertion. After membrane insertion, PilF (pink) may bind and stabilize the outer-barrel of PilQ
610 adjacent to the secretin gate, helping to facilitate secretin oligomerization and transporting PilQ
611 to the outer membrane (OM). TsaP (yellow and brown) might then replace PilF, playing a non-
612 essential accessory role in PilQ assembly. **B,** TsaP binding may cause secretin gate invagination.
613 **C,** TsaP binding to the secretin domain of PilQ and the peptidoglycan could put tension on PilQ
614 stretching. After the pilus has polymerized and then depolymerized, extended PilQ could be
615 contracted by TsaP. **D,** At native expression levels it is not clear what role TsaP plays in the
616 cyclic di-GMP signal cascade. However, over-expressed TsaP triggers the surface sensing cyclic
617 di-GMP signal cascade independent of PilQ.
618

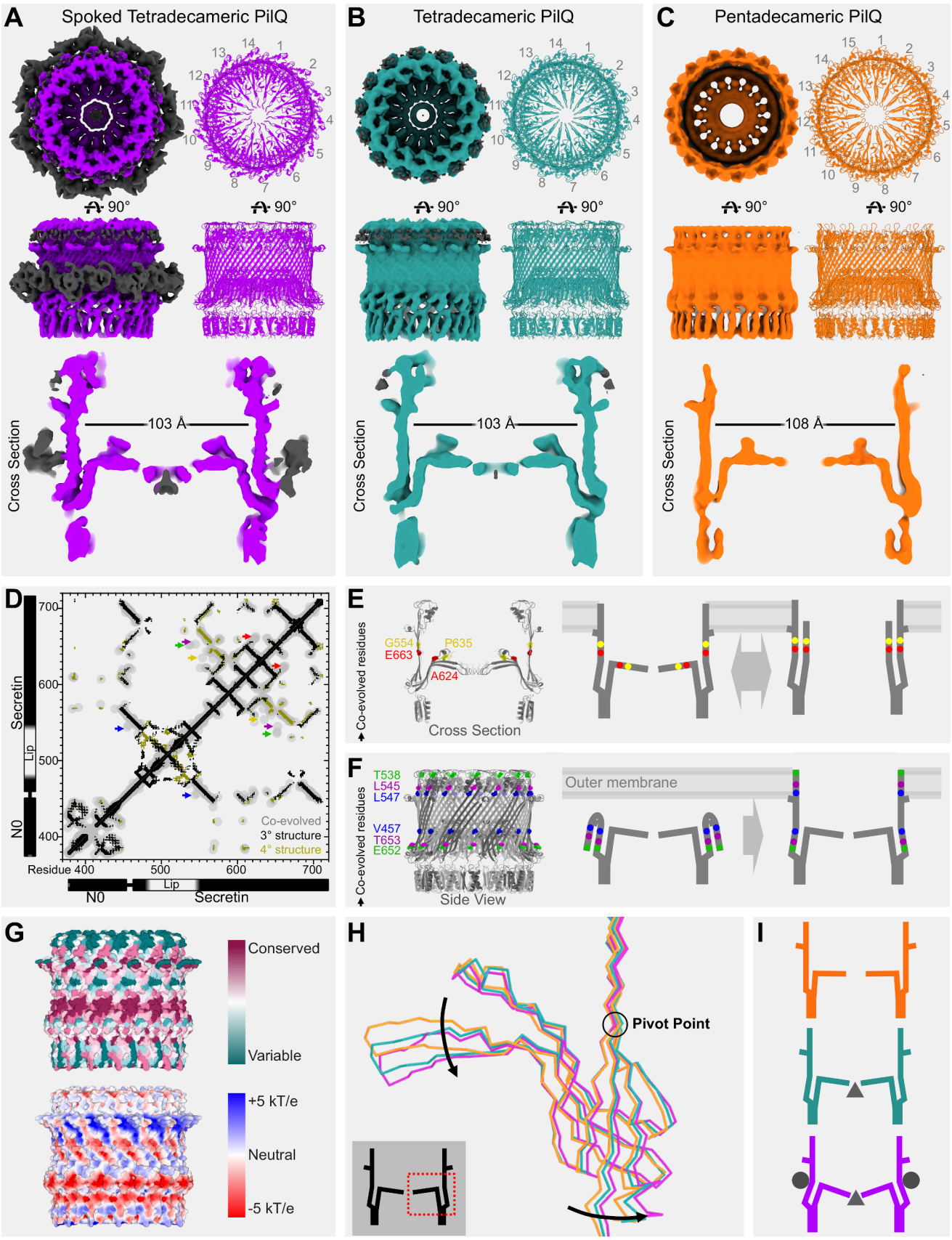
A
Spoked Tetradecameric PilQ
B
Tetradecameric PilQ
C
Pentadecameric PilQ
90°
Cross Section
103 Å
108 Å
D
Secretin
N0
Lip
Co-evolved
3° structure
4° structure
Residue 400
E
Co-evolved residues
G554
E663
P635
A624
Cross Section
F
T538
L545
L547
V457
T653
E652
Side View
Outer membrane
G
Conserved
Variable
+5 kT/e
Neutral
-5 kT/e
H
Pivot Point
I

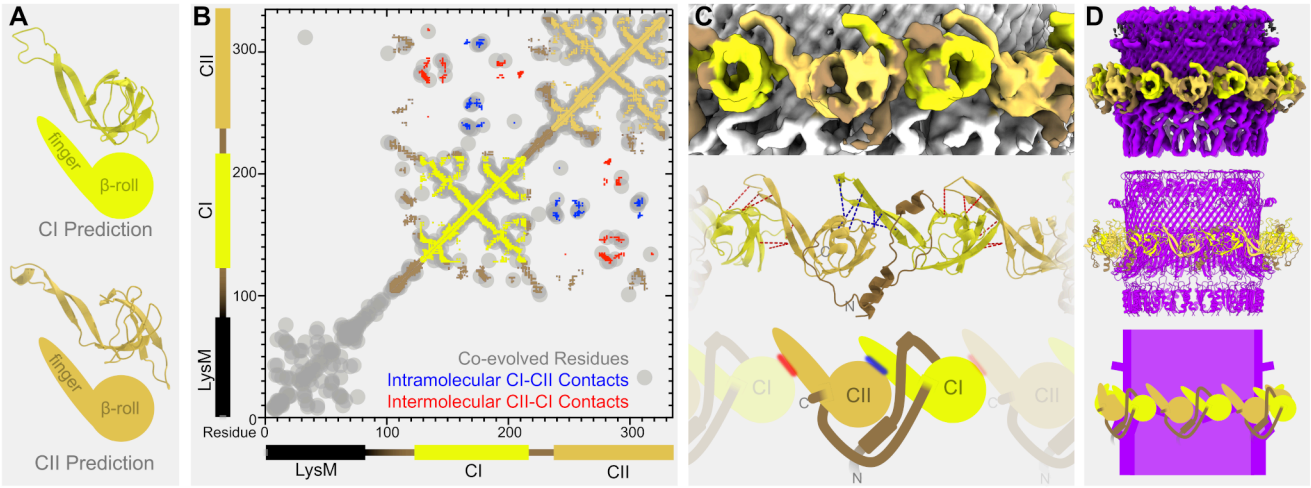
A
finger
β-roll
CI Prediction
finger
β-roll
CII Prediction
B
CII
CI
LysM
300
200
100
0
Residue 0
100
200
300
LysM
CI
CII
Co-evolved Residues
Intramolecular CI-CII Contacts
Intermolecular CII-CI Contacts
C
CI
CII
CI
CII
C
C
N
N
N
D

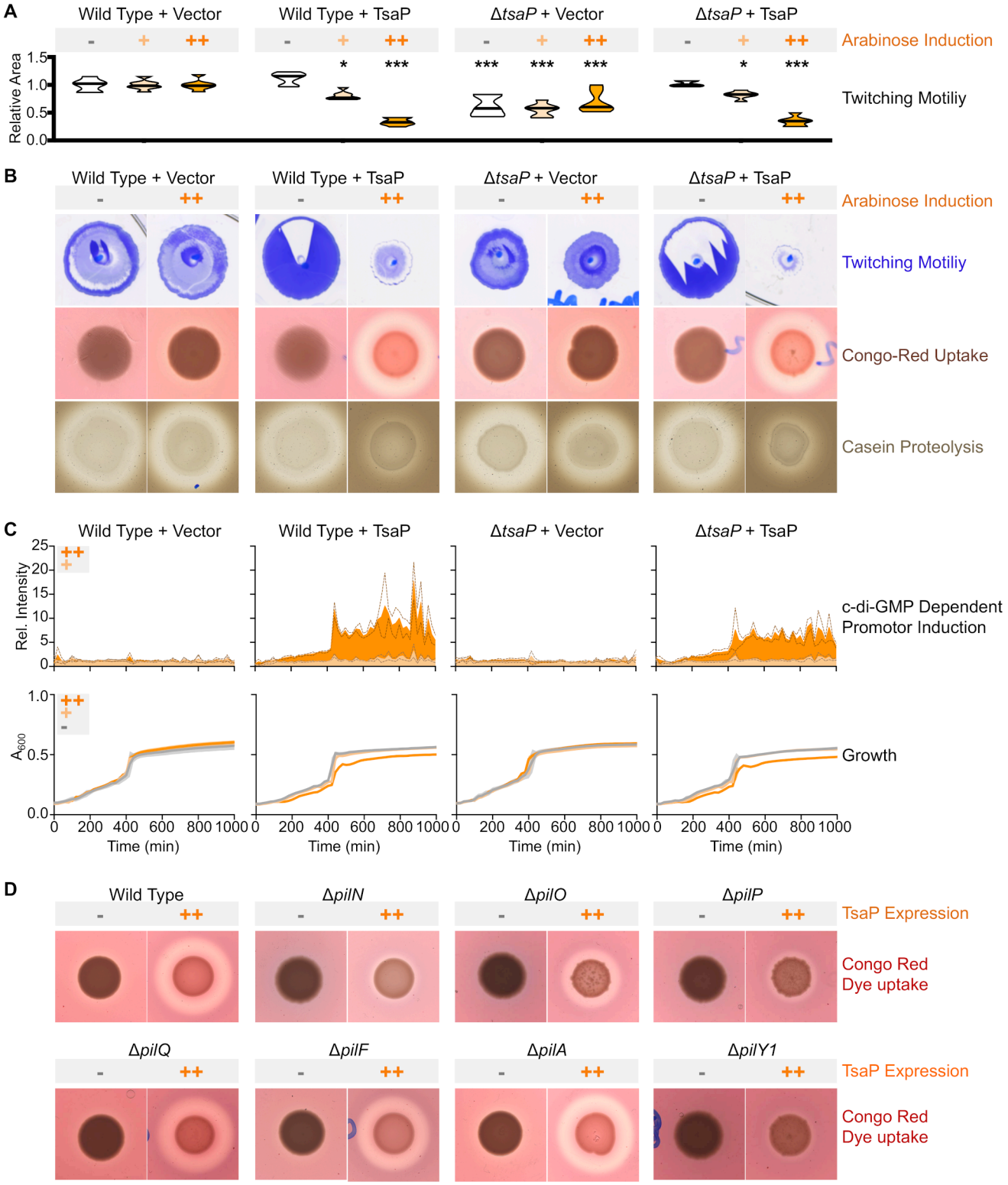
A
Wild Type + Vector
Wild Type + TsaP
ΔtsaP + Vector
ΔtsaP + TsaP
Arabinose Induction
Relative Area
Twitching Motiliy
B
Twitching Motiliy
Congo-Red Uptake
Casein Proteolysis
C
Rel. Intensity
c-di-GMP Dependent Promotor Induction
Growth
Time (min)
D
Wild Type
ΔpilN
ΔpilO
ΔpilP
ΔpilQ
ΔpilF
ΔpilA
ΔpilY1
TsaP Expression
Congo Red Dye uptake

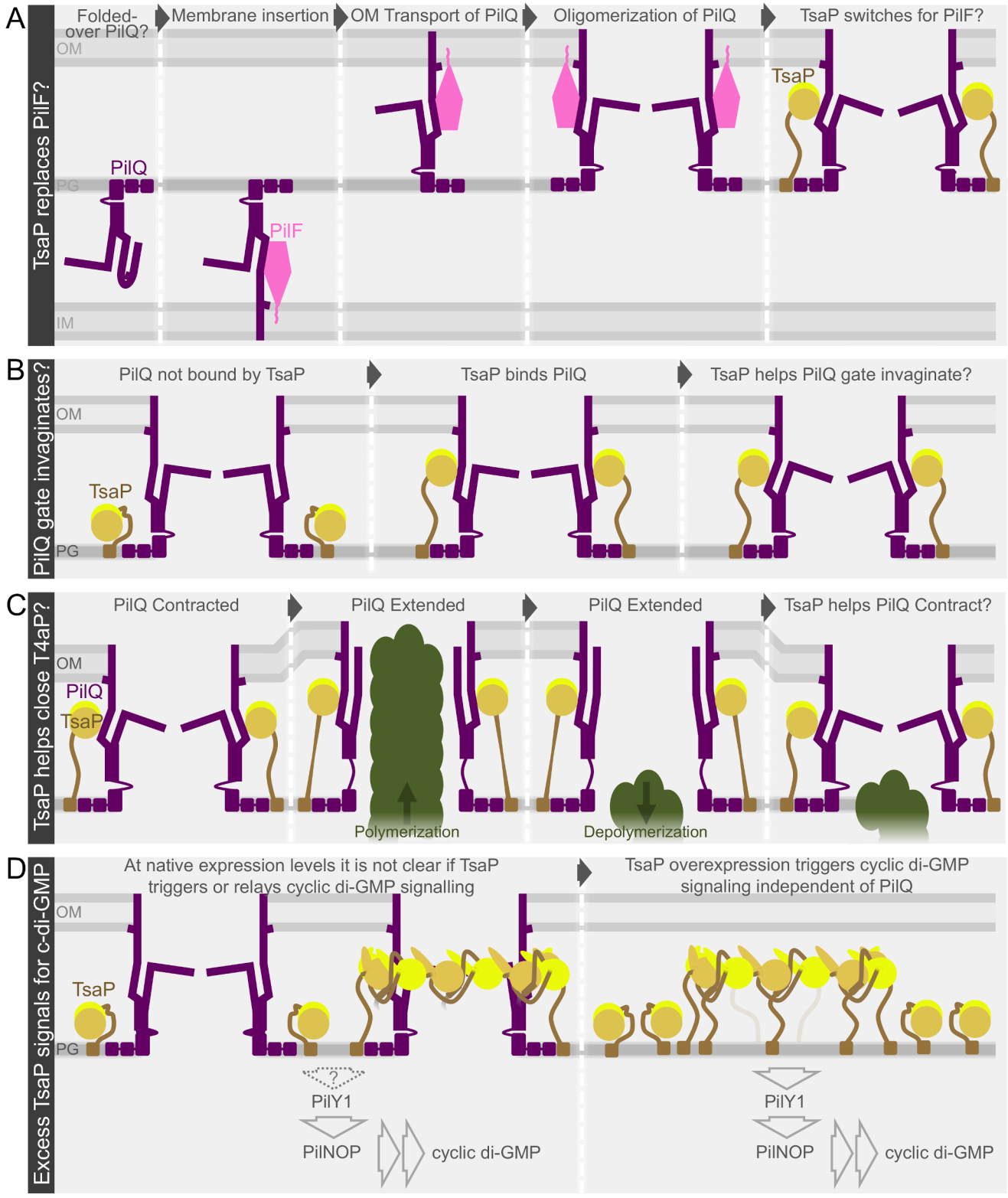
A
TsaP replaces PilF?
Folded-over PilQ?
Membrane insertion
OM Transport of PilQ
Oligomerization of PilQ
TsaP switches for PilF?
OM
PilQ
PG
PilF
TsaP
IM
B
PilQ gate invaginates?
PilQ not bound by TsaP
TsaP binds PilQ
TsaP helps PilQ gate invaginate?
OM
TsaP
PG
C
TsaP helps close T4aP?
PilQ Contracted
PilQ Extended
PilQ Extended
TsaP helps PilQ Contract?
OM
PilQ
TsaP
Polymerization
Depolymerization
D
Excess TsaP signals for c-di-GMP
At native expression levels it is not clear if TsaP triggers or relays cyclic di-GMP signalling
TsaP overexpression triggers cyclic di-GMP signaling independent of PilQ
OM
TsaP
PG
?
PilY1
PilNOP
cyclic di-GMP
PilY1
PilNOP
cyclic di-GMP